Implementing Innovative Ideas in Structural Engineering and Project Management
Edited by Saha, S., Zhang, Y., Yazdani, S., and Singh, A.

ISBN: 978-0-9960437-1-7

IMAGE ANALYSIS BASED FINITE STRAIN MEASUREMENT OF LOCAL DEFORMATION UNDER UNIAXIAL LOAD USING NATURAL STRAIN

YASUYUKI KATO

Dept of Mechanical Engineering, College of Science & Technology, Nihon University, Tokyo, Japan

This paper describes the effectiveness of image analysis based on the Natural Strain theory for measuring the finite strain. Since the additive law of strain on an identical line element can be satisfied and the rigid body rotation can clearly be removed from the shearing strain components, the Natural Strain theory is significantly effective for representing the stress-strain behavior under large elasto-plastic deformation. In this study, the strain measurements under large deformation are conducted by making use of such merits into the image analysis. In our previous studies, in order to verify the effectiveness of this method, the results of strain measurement by image analysis have been compared with the results of conventional strain measurement based on the displacement meter. Consequently, since the results of both measurements almost coincide, the validity of this image analysis has been confirmed. However, these experiments were limited to uniform deformation fields, although in the range of finite deformation. Hence, as for the local deformation, the detailed measurements have not been carried out yet in our previous study. So, in this paper, the local deformations generated under uniaxial tension and simple shear are investigated as the fundamental research. Especially, the progress of local deformations is revealed by comparing the measured values of upper and middle positions in the specimen.

Keywords: Elasto-plastic analysis, Local deformation, Optical image processing, Uniaxial tension, Simple shear, Line elements.

1 INTRODUCTION

In general, the electrical measurements such as displacement meter and strain gauge etc. are widely adopted for the strain measurement. Among these measurements, in the case of displacement meter, there is a limitation in the measuring range and accuracy. And, in case of the measurements by strain gauge, there is the possibility of detachment of strain gauges during measurements, and also in this case, there is a limitation in the measuring range. On the other hand, the strain measurement based on the image analysis can be measured continuously over a wide range from the infinitesimal deformation up to the large deformation. Thus, the strain measurement based on the image analysis is highly effective method for representing the elasto-plastic behavior under large deformation. Therefore, in this study, we take up the strain measurement by image analysis as the theme of this research, and reveal the

effectiveness of the image analysis based on the Natural Strain theory. Here, the Natural Strain theory used in this study is the finite strain representation, which is obtained by integrating the strain rate on an identical line element over a whole process of deformation path. And as the result, the extensional strain component is represented as a logarithm of the ratio of current length to undeformed length of a line element. On the other hand, the shearing strain component becomes pure angular strain, which is obtained by removing the rigid body rotation from the rotating angle of a line element. Since the additive law of strain on an identical line element can be satisfied, this strain is possible to represent the strain from anywhere, with reference to the deformed intermediate state. Therefore, in this study, we proceed with our research by making use of the merit of Natural Strain theory into the image analysis effectively.

In the series of our previous studies (Kato and Futami 2013), three types of different deformation history, i.e., the proportional loading of tension and shear, the shear after applying tension and the tension after applying shear, were examined. Then, strain measurements based on the image analysis have been compared with measurements by conventional displacement meter, and the validity of this method has been confirmed. However, these experiments were limited to uniform deformation fields, although in the range of finite strain. Thus, the detailed measurements of the local deformation, which arises after the uniform deformation fields, have not been conducted yet in our previous study.

So, we take up the local deformation generated under uniaxial loading states of tension and simple shear as the next research themes. In this study, measurements based on image analysis are compared with measurements by displacement meter within the range of large deformation that the local deformations arise. In addition, in order to clarify the progress of local deformation, measurements of image analysis at upper and middle position in the test specimen is also compared in this study.

2 MESUREMENT METHOD OF PRINCIPAL STRAIN AND ITS DIRECTION

The methods of image analysis for deriving principal strain and its direction are described in this chapter. The three line elements ℓ_{oa}, ℓ_{ob}, ℓ_{oc} which is located at arbitrary directions β_{oa}, β_{ob}, β_{oc} are shown in Figure 1. Here, in the case of a line element ℓ_{oa}, the relation between original undeformed state and deformed current state can be derived as:

$$\ell_a = \boldsymbol{D}\,\ell_{oa} = \begin{bmatrix} D_{11} & D_{12} & 0 \\ 0 & D_{22} & 0 \\ 0 & 0 & D_{33} \end{bmatrix} \begin{bmatrix} \| \ell_{oa} \| \cos\beta_{oa} \\ \| \ell_{oa} \| \sin\beta_{oa} \\ 0 \end{bmatrix} \tag{1}$$

The extensional strain component for Natural Strain theory is represented as follows.

$$\varepsilon_a = \frac{1}{2} ln\left(\frac{\ell_a{}^T \ell_a}{\ell_{oa}{}^T \ell_{oa}} \right) = \frac{1}{2} ln\left(\frac{\ell_{oa}{}^T \boldsymbol{D}^T \boldsymbol{D} \ell_{oa}}{\ell_{oa}{}^T \ell_{oa}} \right) = \frac{1}{2} ln\left(D_{11}{}^2 cos^2\beta_{oa} + 2D_{11}D_{12} sin\beta_{oa} cos\beta_{oa} + D_{12}{}^2 sin^2\beta_{oa} + D_{22}{}^2 sin^2\beta_{oa} \right) \tag{2}$$

Similarly, ε_b and ε_c can be derived. Hence, the following relation is derived.

$$\begin{bmatrix} D_{11}{}^2 \\ D_{11}D_{12} \\ D_{12}{}^2 + D_{22}{}^2 \end{bmatrix} = \begin{bmatrix} \cos^2\beta_{oa} & 2\sin\beta_{oa}\cos\beta_{oa} & \sin^2\beta_{oa} \\ \cos^2\beta_{ob} & 2\sin\beta_{ob}\cos\beta_{ob} & \sin^2\beta_{ob} \\ \cos^2\beta_{oc} & 2\sin\beta_{oc}\cos\beta_{oc} & \sin^2\beta_{oc} \end{bmatrix}^{-1} \begin{bmatrix} \exp(2\varepsilon_a) \\ \exp(2\varepsilon_b) \\ \exp(2\varepsilon_c) \end{bmatrix} \tag{3}$$

If we consider the special case when the line element ℓ_{oa} is fixed on the base surface in the initial state, i.e., $\beta_{oa} = 0$, $\beta_{ob} = \beta_{oa} + \pi/4$, $\beta_{oc} = \beta_{oa} + \pi/2$, the components of the deformation gradient tensor are represented as follows.

$$D_{11} = \exp(\varepsilon_a) \tag{4}$$

$$D_{12} = \exp(2\varepsilon_b - \varepsilon_a) - \frac{1}{2}\left(\exp(\varepsilon_a) + \exp(2\varepsilon_c - \varepsilon_a)\right) \tag{5}$$

$$D_{22} = \sqrt{\exp(2\varepsilon_c) - \left\{\exp(2\varepsilon_b - \varepsilon_a) - \frac{1}{2}\left(\exp(\varepsilon_a) + \exp(2\varepsilon_c - \varepsilon_a)\right)\right\}^2} \tag{6}$$

The principal value of strain ε_1 and its direction θ_m are determined from the polar decomposition of deformation gradient, and these are represented as follows.

$$\varepsilon_1 = \ln \lambda_1 = \ln \left\{ \frac{\sqrt{D_{11}{}^2 + D_{12}{}^2 + D_{22}{}^2 + 2D_{11}D_{22}} + \sqrt{D_{11}{}^2 + D_{12}{}^2 + D_{22}{}^2 - 2D_{11}D_{22}}}{2} \right\} \tag{7}$$

$$\theta_m = \frac{\pi}{4} - \frac{1}{2} \tan^{-1}\left\{ \frac{D_{11}{}^2 + D_{12}{}^2 - D_{22}{}^2}{2D_{12}D_{22}} \right\} \tag{8}$$

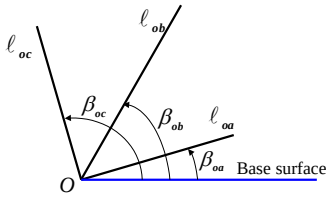

Figure 1. Three line elements in a plane.

3 EXPERIMENTAL METHOD

3.1 Experimental Equipment and Test Specimen

The multi-axial loading test machine, which can be applied tension and torsion, are used in the experiments, and the cylindrical specimens made of annealed pure copper, purity 99.99% (the initial mechanical properties are shown in Table 1), are adopted, and the outside diameter, the inside diameter and the gauge length of these specimens are 22 [mm], 16 [mm] and 30 [mm], respectively.

Table 1. Mechanical properties of specimen.

Young's modulus E [MPa]	Shear modulus G [MPa]	Yield stress σ_Y [MPa]	Yield stress τ_Y [MPa]	Poisson' ratio ν [-]
116,700	43,800	13.8	8.0	0.33

3.2 Experimental Conditions

In this study, two types of deformation path, i.e., (a) the uniaxial tension, in which the maximum elongation is 13.6 [mm], (b) the simple shear, in which the maximum torsional angle 500 [deg.], are carried out.

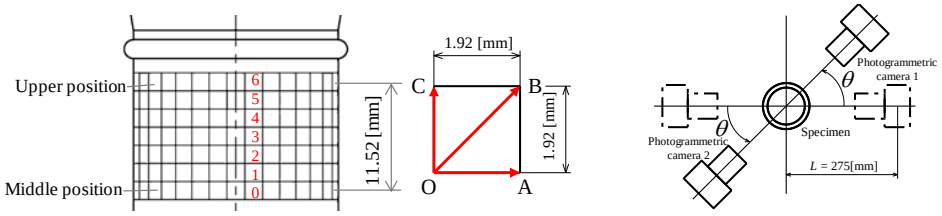

(a) Specimen (b) Position of cameras

Figure 2. Specimen and camera.

4 EXPERIMENTAL RESULTS

4.1 Experimental Results of Uniaxial Tension

Figure 3 shows an example of photographic image obtained in each element. In these figures, (i) and (ii) mean photographs taken at upper and middle position in the test specimen. Here, (i-A) and (ii-A) are photographs taken at 117 [MPa] (deviatoric stress). And, (i-B) and (ii-B) are photographs at 185 [MPa], (i-C) and (ii-C) are photographs at 202 [MPa], respectively. From comparison of these photographic imagery, since there is no great distinction between deformation of image (i) and deformation of image (ii) until 185 [MPa], the uniform deformation is produced in the specimen. On the other hand, from the comparison of image (i-C) and (ii-C), it can be seen that the tensile deformation in image (ii-C) is advanced compared with deformation in image (i-C).

Next, Figure 4(i) shows the deviatoric principal stress-deviatoric principal strain curve measured at the upper position in the test specimen. In this figure, square plots □ represent measurements by image analysis and the solid plots ◆ are measurements by ordinary displacement meter. The A, B, C in the figure are corresponding to each location where the photographs in Figure 3 were taken. In a relatively early stage of measurement, it can be seen that both measurements are good agreement with each other. However, differences between measurements based on the image analysis and measurements by ordinary displacement meter begin to occur at point B in the figure, and at point C, measurements based on the image analysis become smaller value compared to measurements by ordinary displacement meter. On the other hand, Figure 4 (ii) shows the deviatoric principal stress-deviatoric principal strain curve measured at the middle position in the test specimen. In this figure, circular plots ○ represent

measurements by image analysis. At point C, measurements based on the image analysis become larger value than measurements by ordinary displacement meter.

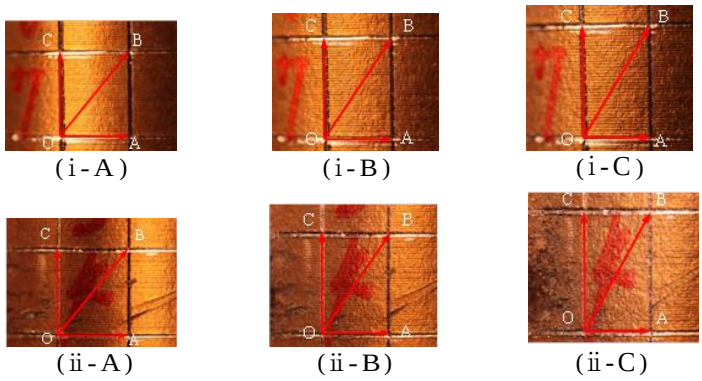

Figure 3. Comparison of photographs in uniaxial tension.

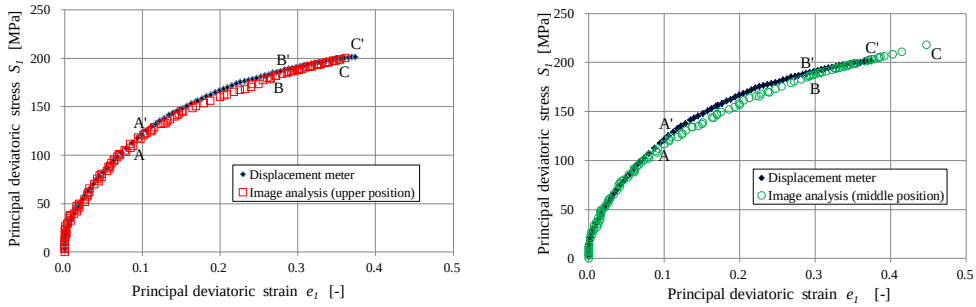

(i) Upper position (ii) Middle position

Figure 4. Deviatoric principal stress- principal strain curve (uniaxial tension).

4.2 Experimental Results of Simple Shear

Figure 5 shows an example of the photographs of image data. Here, (i-A) and (ii-A) are photographs taken at 143 [MPa] (shear stress). (i-B) and (ii-B) are photograph taken at 169 [MPa], (i-C) and (ii-C) are photograph taken at 184 [MPa], respectively.

Figure 6(a) shows the deviatoric principal stress- deviatoric principal strain curve. Here, square plots □ represent measurements at upper position, circular plots ○ represent measurements at middle position. The A, B, C in this figure are corresponding to each location where the image data in Figure 5 was taken. It can be confirmed that both measurements are good agreement with each other until point B, which is much larger compared to the deformation when local deformations arise in the uniaxial tension. However, it can be seen that measurement results of upper position and middle position become different values at point C. Next, in order to examine the progress of local deformation at point C quantitatively, the difference between the principal strain in each element e_{1i} and the principal strain by

displacement meter e_{1d}, i.e., $\Delta e_1 = e_{1i} - e_{1d}$, is investigated. Figure 6(b) shows the relation between the difference of principal strain Δe_1 and the number of element *N*. It can be confirmed from this figure that local deformations are generated along the longitudinal direction in the test specimen.

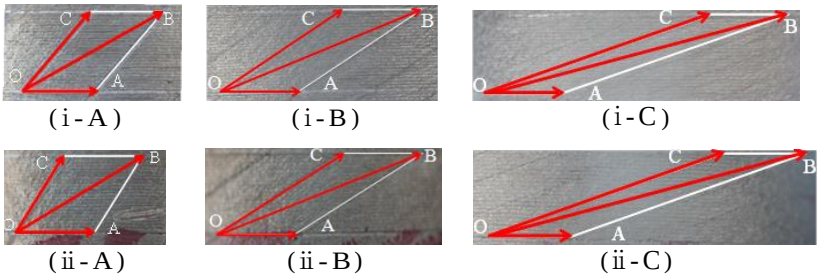

Figure 5. Comparison of photographs in simple shear.

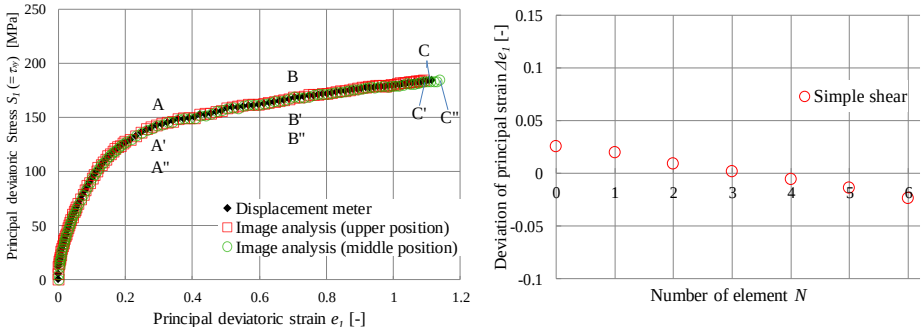

(a) Upper and middle position. (b) Deviation of principal strain in load C.

Figure 6. Deviatoric principal stress-principal strain curve (simple shear).

5 CONCLUDING REMARKS

The finite strain measurement by image analysis under uniaxial tension and simple shear was carried out on the basis of the Natural Strain theory, and measurements by image analysis were compared with measurements by the conventional displacement meter in the range of large deformation that the local deformations arise. And as the result, in the case of uniaxial tension, it was revealed that the measurement result becomes the smallest value at the upper position in the test specimen and becomes the largest value at the middle position. On the other hand, in the case of simple shear, it could be confirmed that local deformations arise under more large deformation compared to the case of uniaxial tension.

References

Kato, Y., and. Futami, M., Finite Strain Measurement Based on Image Analysis using Natural Strain (Measurement and Evaluation in Uniform Deformation Field), *New Developments in Structural Engineering and Construction*, *Vol 1*, Yazdani, S. and Singh, A. (eds.), 171-176, Research Publishing Services, Singapore, 2013.